INTERFACE

royalsocietypublishing.org/journal/rsif

Research

Cite this article: Ko H, Hu DL. 2020 The physics of tossing fried rice. *J. R. Soc. Interface* **17**: 20190622.
http://dx.doi.org/10.1098/rsif.2019.0622

Received: 5 September 2019
Accepted: 15 January 2020

Subject Category:
Life Sciences–Physics interface

Subject Areas:
biophysics

Keywords:
biophysics, granular material, dynamics

Author for correspondence:
David L. Hu
e-mail: hu@me.gatech.edu

Electronic supplementary material is available online at https://doi.org/10.6084/m9.figshare.c.4828269.

THE ROYAL SOCIETY PUBLISHING

The physics of tossing fried rice

Hungtang Ko[1] and David L. Hu[1,2]

[1]Schools of Mechanical Engineering, and [2]School of Biology, Georgia Institute of Technology, Atlanta, GA 30332, USA

HK, 0000-0001-6250-6144; DLH, 0000-0002-0017-7303

Fried rice is a 1500-year-old dish that is prepared using wok tossing, a technique that enables food to undergo temperatures of 1200°C without burning. Tossing of the heavy wok at high speed may be one contributor to shoulder pain, which is reported by 64.5% of Chinese restaurant chefs. In this combined experimental and theoretical study, we report the wok tossing kinematics of five professional restaurant chefs. The wok toss has a period of 0.3 s and involves two directions of movement: translation, which slides the rice along the wok, and rotation, which throws the rice into the air. We report the chosen kinematics of the chefs and use a theoretical model to predict the trajectory of rice based on projectile motion. Using our model, we rank all possible kinematics in terms of three metrics: the proportion of the rice that is tossed, its flight height and the angular displacement of the rice. We identify an optimal regime for making fried rice and suggest ways that wok tossing may be improved. This study may inspire the design of stir-fry robotics and exoskeletons to reduce the rate of muscle strain injury among professional chefs.

1. Introduction

Stir-frying was used originally for drying rather than cooking food in the Han dynasty (206 BC to AD 220) [1]. One of the most popular dishes to emerge from this technique was *scattered golden rice*, which originated 1500 years ago in the Sui dynasty (581–619 AD) [2]. Stir-frying provides the long-sought wok hei flavour or *the breath of the wok* [3]. Wok hei is a type of browning, enabled by the Maillard [4] chemical reaction that takes place only when the wok surface reaches 1000°C. Under such high temperatures, chefs [5] surmise that the rapid motion of the wok enables browning without burning. This idea, however, has not yet been tested quantitatively. The goal of this study is to determine the mechanics underlying wok motion that makes browning without burning possible.

By studying wok tossing kinematics, we hope to improve the process of frying rice and inspire exoskeletons to reduce injuries in the restaurant industry. Fried rice is made in most of the Asian cuisines. In Chinese restaurants, it is made with the wok, the weight and speed of which have long been suspected to play a role in the high injury rate among chefs. Wok tossing is frequently mentioned in the literature concerning musculoskeletal disorders among Chinese chefs [6–8]. In 2014, wok tossing was highlighted as one of several critical risk factors that call for investigation and immediate change [6]. The precise muscles that are used in wok tossing remain unknown, but it is likely that the shoulder is heavily relied upon. The shoulder is used in a number of restaurant activities, and, as a consequence, discomfort of the shoulder is the most common disorder among Chinese restaurant chefs, with a prevalence of 64.5% [9]. Shoulder discomfort has forced two out of 18 chefs to leave their jobs [7]. Understanding the kinematics of the wok is an important first step in understanding how wok tossing affects the body.

Since the 1950s, there has been interest in the automation of cooking. Recent cooking robotics research has focused mostly on using humanoid robots to mimic human kitchen activities, such as cutting, boiling, frying and moving ingredients [10–13]. For dynamic tasks such as pancake-flipping, robots use an advanced reinforcement learning algorithm to learn the task [10]. In

industry, the automation of stir-frying has been attempted, but the quality of the cooked food still cannot match that of human counterparts. Most stir-fry designs use rotating [14], stirring [15,16] or shaking [17–19] to mix the ingredients. In 1957, Wang [14] invented a stir-fry robot that mixes the ingredients using a rotating drum whose axis is oblique to the floor. Later in the 1980s, designs included automated stirring implements such as spatulas [15,16]. In the 1990s, engineers combined these approaches to build a see-sawing wok that flips materials like a pancake and then uses an automated spatula to prevent them from sticking [17–19].

Automation has reached a point such that some restaurants predominantly use robots to prepare food [20]. Spyce is a restaurant based in Boston, MA, USA, that uses rotating drums to mix and heat Chinese food at frequencies of 0.5 Hz, which, as we will see, is six times less than the wok tossing of professional chefs. The low speed reduces the jumping of the food, and likely precludes the high temperatures that permit the Maillard reaction. The machine that best mimics professional chefs is the stir-fry machine showcased in 2014 at the restaurant Ruyi at Changi Airport, Singapore [21]. Yet even it moves at a frequency of 2 Hz, which is still too low to enable airborne motion of food.

In this paper, we will introduce a mathematical model for wok tossing based on the kinematics of professional chefs. We begin in §2 with our methods for filming and analysing the videos of professional chefs. In §3, we present our theoretical model and numerical methods for estimating the results of the model. In §4, we compare our experimental results with those of the theory. We follow in §5 with a discussion of the repercussions and application of this work and conclude in §6.

2. Material and methods

2.1. Filming professional chefs

We filmed a total of five chefs from Taiwan and China. In the summer of 2018, one video was taken from the Ruyi stir-fry restaurant in Chulu, Taiwan, and two videos were taken from the Pinxin stir-fry restaurant in Nanwang, Taiwan. The chefs were the owners of the restaurants and each had more than 20 years of cooking experience. Moreover, these restaurants specialize in stir-fry cuisines. To obtain further data on the frequency of wok tossing, in the summer of 2019, we used a mobile phone (Huawei Mate 9) to film cooking in Henan Province, China. The three restaurants filmed were Xiao Chuan Er, Ma La Xiang Guo and Da Rong He. We recorded chefs cooking different stir-fry dishes and extracted the frequency data using ImageJ. Documentation of our recordings may be found in the electronic supplementary material.

At the Taiwanese restaurants, we used two Sony HDR-PJ675 cameras with a 60 fps recording rate to record the cooking. One camera filmed the wok from the side while the other filmed from above the chef's shoulder. The iron wok used by the chefs weighed 1.4 kg and was 39 cm wide and 13 cm deep. The chefs cooked one serving of their regular fried rice on the menu, which contained rice, eggs, pork, carrot and corn as the main ingredients. One serving of the completed dish weighed around 0.3 kg.

The films contained a total of 276 cycles of wok tossing. The cooking process typically lasted 2 min, which included steps such as preheating the wok, sequentially adding the ingredients, mixing with a spatula and wok tossing. During these steps, wok tossing was sporadic. However, after the chef added all the ingredients, wok tossing lasted for at least five consecutive cycles. The chefs would occasionally use the spatula to prevent individual rice grains from sticking onto the wok. For the purpose of fitting parameters and performing Fourier transformation, we analysed a video segment featuring 17 consecutive cycles after all the ingredients had been added. In addition, to show that the tossing frequency we observed may be applied to more general situations, we recorded the chef in Taiwan tossing the wok with three servings of fried rice at the same time.

2.2. Video analysis

We re-encoded the videos using the free multimedia conversion tool FFmpeg. Then, the video was fed into the open-source image-processing tool ImageJ [22] with the plugin Manual Tracking. In the videos, the wok is oriented horizontally, with the handle on the right. The width of the wok is used to calibrate the length scale in the videos. Then, we manually tracked the trajectories of the left and right endpoints of the wok. The right rim of the stove was selected as the origin of the kitchen coordinate because the wok remains in contact with this point.

The wok bottom surface has a constant radius of curvature $L = 20$ cm, a width $W = 37$ cm and a depth $D = 13$ cm. A definition of the dimensions is shown in figure 2*b*. We consider a single plane that bisects the wok and intersects the wok handle. Since the wok handle moves within this plane, so too do the points of interest on the wok. The points of the wok that intersect the plane are points on a circle of radius L. We refer to the centre of the circle as the wok centre, shown by the red point in figure 2*b*. Note that this point differs from the work centre of mass. Locations on the wok may be parameterized using the angle ζ from the middle of the wok, as shown in green in figure 2*b*. Thus, $\zeta = 0$ denotes the middle of the wok, and $\zeta = -\zeta_{\max}$ and $\zeta = \zeta_{\max}$ are the leftmost and rightmost ends of the wok, respectively, where our wok has the angle $\zeta_{\max} = 1.2$ rad or 70°. $\zeta_{\max}$ is a simple representation of the wok shape. It is directly related to the width W, depth D and radius L through trigonometry: $L = \frac{W}{2\sin\zeta_{\max}} = \frac{W\tan(\zeta_{\max})}{2} + D$. For most of our work, we will assume this particular wok shape, but later we will consider the effect of different wok shapes.

The wok centre was measured in each video frame using the following geometrical considerations. In each snapshot, we first measured the coordinates of the left end $\boldsymbol{R}_l = [x_l, y_l]$ and the right end $\boldsymbol{R}_r = [x_r, y_r]$. These coordinates are used to calculate the unit vector that is normal to the line segment connecting both ends of the wok. The unit normal vector of the wok $\hat{n}_{\text{wok}}$ was calculated by normalizing $[y_l - y_r,\ x_r - x_l]$. The location of the wok centre may be calculated by adding the difference between the wok radius L and the wok depth D to the midpoint of the wok ends: $\boldsymbol{R}_c = (1/2)(\boldsymbol{R}_l + \boldsymbol{R}_r) + (L - D)\hat{n}_{\text{wok}}$. The trajectories of the left and right ends $\boldsymbol{R}_l$ and $\boldsymbol{R}_r$ are shown in blue and the trajectory of the wok centre $\boldsymbol{R}_c$ is shown in red in figure 1*b–e*.

3. Mathematical modelling

The goal of the model is to predict the airborne trajectories of the rice based on the kinematics of the wok. Our experiments indicate that the wok is moved in two dimensions; furthermore, the wok motion may be described by two degrees of freedom.

3.1. Wok kinematics

Since the wok is heavy, human chefs rarely lift the wok off the stove, but instead maintain a single sliding point of contact. This constraint enables us to model the wok position and angle with a theoretical two-link pendulum. The pendulum

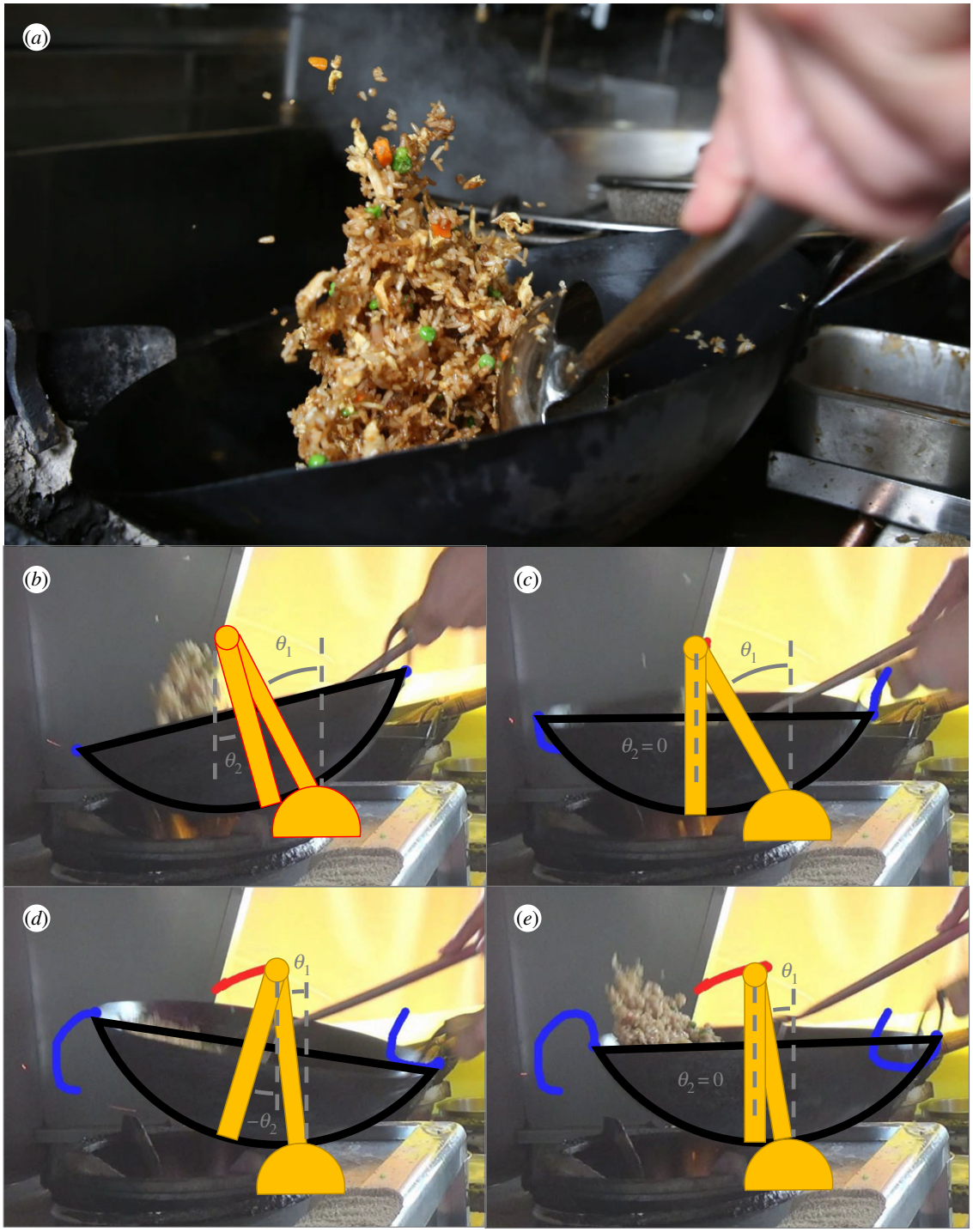

Figure 1. Kinematics of tossing fried rice. (*a*) Wok tossing at the Chin Chin restaurant in Atlanta, GA, USA. Photo credit: Candler Hobbs. (*b–e*) Image sequence showing the wok tossing process. The coloured points show several points tracked in the video. Note that the left rim travels in a clockwise circle and the right rim in a counterclockwise circle. Both trajectories are marked in blue while the trajectory of the wok centre is marked in red. Our two-link pendulum model is overlaid on top of the image sequence to show the evolution of the model variables θ_1 and θ_2.

is imaginary, but it enables the wok's motion to be modelled using only two variables. The first link of the pendulum is fixed to the stove at the wok's point of contact, and the second link is fixed to the wok, as shown in figure 2*a*. The length of both links is set to the radius of the wok L in order to satisfy the constraint that the wok and the stove remain touching.

We proceed by defining several variables that govern the wok kinematics. The joint between the links has the same position as the wok centre, $\boldsymbol{R}_c$. The first and second links have two independent angles $\theta_1(t)$ and $\theta_2(t)$, respectively, with respect to the vertical direction. Physically, θ_1 determines the location of the wok centre while θ_2 determines the orientation of the wok, as can be seen in figure 1*b–e*. Moreover, $\zeta_{\text{contact}} = \theta_2 - \theta_1$ represents the angular coordinate of the point on the wok that touches the stove.

We calculated the time course of $\theta_1(t)$ and $\theta_2(t)$ from our videos of wok tossing. If the wok centre is at $[x_c, y_c]$, the angle θ_1 may be written as $\theta_1 = \arctan((-x_c)/(y_c))$. The angle $\theta_2(t)$ is equal to the inclination angle of the wok: $\theta_2 = \arctan((y_r - y_l)/(x_r - x_l))$ at each time instant. The time courses of the angles are shown in figure 2*c* and are well

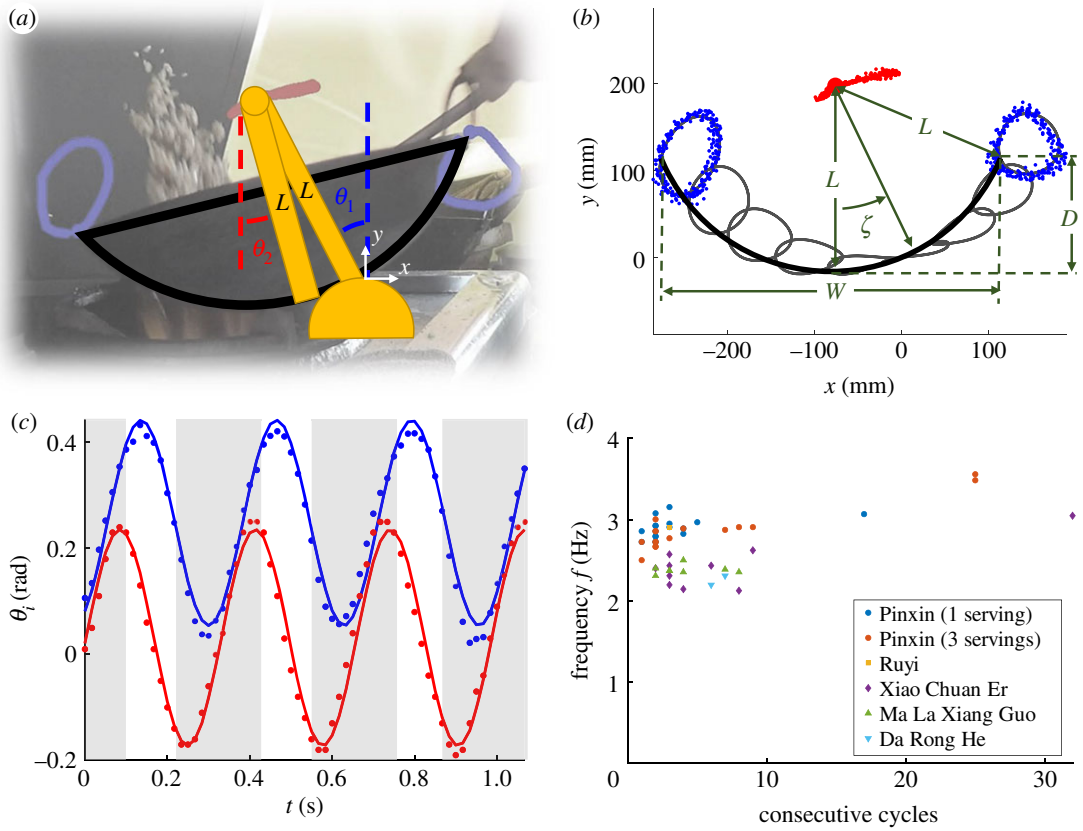

Figure 2. Mathematical model of wok tossing. (*a*) Schematic diagram showing the mathematical model. (*b*) The trajectories of set points on the wok, plotted in grey in the kitchen coordinate frame. Experimental data are shown by the blue solid points and the simulation is shown by the grey lines. The left- and rightmost points of the wok coincide well with the simulation. The green lines define the wok parameters. The angle ζ characterizes the position on the wok, which varies from $-\zeta_{max}$ to ζ_{max}. Constants L, D and W mark the radius, the depth and the width of the wok, respectively. (*c*) The angles of the pendulums, θ_1 (red) and θ_2 (blue). Points denote the experiments and lines denote the model. Grey areas represent the airborne phase of the rice. (*d*) Tossing frequency of five professional chefs when stir-fry dishes were cooked. Different colours indicate different chefs.

fitted by the following offset harmonic function:

$$\theta_i(t) = \bar{\theta}_i + A_i \cos(2\pi f t + \phi_i), \tag{3.1}$$

where $i = 1$ or 2, $\bar{\theta}_i$ is the offset of the centre of the signal, A_i is the amplitude of the oscillation, f is the frequency and ϕ_i is the phase angle. Without any loss of generality, we set $\phi_1 = 0$ and $\phi_2 = \phi$. The point of contact with the stove denotes the base of pendulum 1. We set this location as the origin of our Cartesian coordinate system so that $\boldsymbol{R}_{contact} = [0, 0]$. Using geometrical considerations, we can express the Cartesian coordinates of any position ζ on the wok as a function of time t as

$$\boldsymbol{R}_{wok}(\zeta, t) = L\Big[-\sin\theta_1(t) + \sin(\theta_2(t) + \zeta),\ \cos\theta_1(t) - \cos(\theta_2(t) + \zeta)\Big]. \tag{3.2}$$

This completes the kinematic description of the wok. To recover the trajectories of the wok ends $\boldsymbol{R}_l(t)$ and $\boldsymbol{R}_r(t)$, one can simply set ζ to the extreme values in equation (3.2), i.e. $\boldsymbol{R}_l(t) = \boldsymbol{R}_{wok}(-\zeta_{max}, t)$ and $\boldsymbol{R}_r(t) = \boldsymbol{R}_{wok}(\zeta_{max}, t)$. We also check our calculations by showing that, at all points in time, there is some angle $\zeta_{contact}$ at which the wok touches the stove: $\boldsymbol{R}_{wok}(\zeta_{contact}) = 0$.

3.2. Rice trajectories

Now that the kinematics of the wok have been defined, we use simulation to predict the trajectories of rice based on projectile motion. Our goal is to calculate their new landing position $\zeta_{landing}$ based on their initial launch point $\zeta_{take\text{-}off}$ and the kinematics of the wok.

To do this, we must first define the take-off condition to determine the timing of take-off for each rice grain. We consider the normal vector of the wok pointing inwards towards the wok centre $\boldsymbol{n}(\zeta, t)$. Note that the normal vector is a function of both the wok location ζ and time t. It may be calculated by normalizing the vector that points from the wok surface to the wok centre,

$$\boldsymbol{n}(\zeta, t) = \frac{\boldsymbol{R}_c(t) - \boldsymbol{R}_{wok}(\zeta, t)}{|\boldsymbol{R}_c(t) - \boldsymbol{R}_{wok}(\zeta, t)|}, \tag{3.3}$$

where, by geometry, the wok centre may be expressed in model parameters as $\boldsymbol{R}_c(t) = L[-\sin\theta_1(t),\ \cos\theta_1(t)]$.

If the rice is detached from the wok, right after take-off at $t + \Delta t$, the vector pointing from the jumping site to the rice grain should have some component in the normal direction of the wok. The rigorous description of this may be written as

$$\Big(\boldsymbol{R}_{grain}(\zeta, t + \Delta t) - \boldsymbol{R}_{wok}(\zeta, t + \Delta t)\Big) \cdot \boldsymbol{n}(\zeta, t + \Delta t) > 0. \tag{3.4}$$

It is trivial that, at the moment of take-off, $(\boldsymbol{R}_{grain}(\zeta, t) - \boldsymbol{R}_{wok}(\zeta, t)) = 0$. Additionally, we assume that, at the instant of rice take-off, the rice grains have the same normal velocity as the wok: $(\boldsymbol{R}'_{grain}(\zeta, t) - \boldsymbol{R}'_{wok}(\zeta, t)) \cdot \boldsymbol{n}(\zeta, t) = 0$. Therefore, we find that, after doing a Taylor expansion of the first term in equation (3.4), the second derivative term takes the leading order. Taking the limit as Δt goes to zero, we may derive the take-off condition

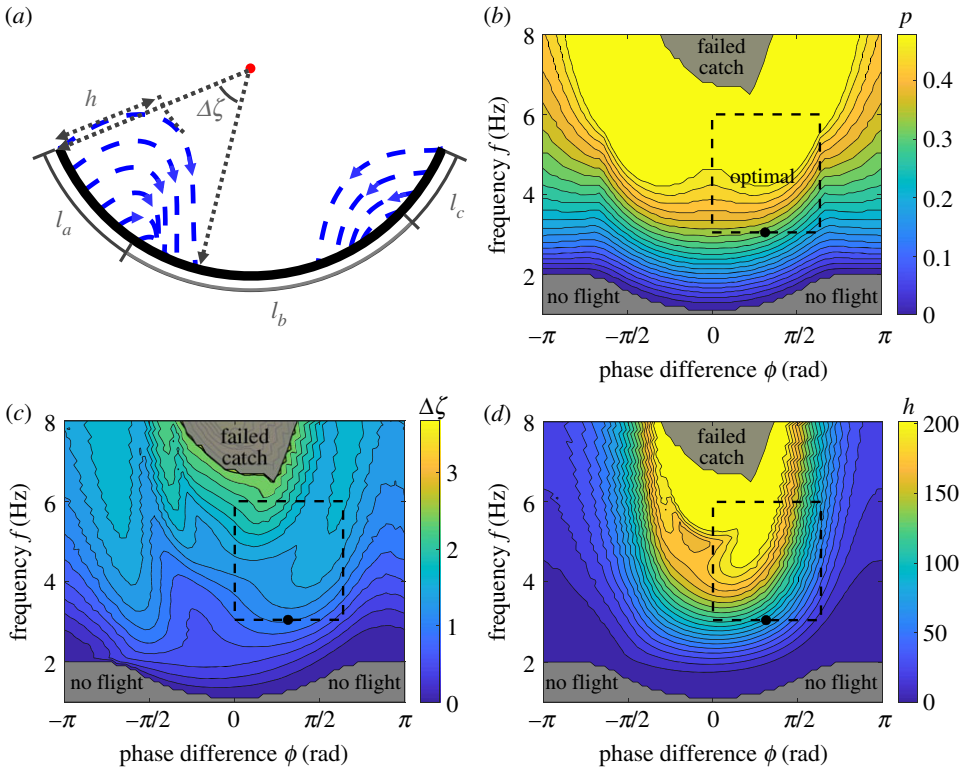

Figure 3. Metrics for evaluating wok tosses. (*a*) Schematic defining the metrics, including the proportion of rice going airborne p, the angular displacement $\Delta\zeta$ (rad) and the flight height h (mm). (*b–d*) Phase diagrams for p, $\Delta\zeta$ and h as phase difference ϕ and frequency f vary. All rice grains remained attached in the 'no flight' zone while the furthest jumping grains could not be caught by the wok in the 'failed catch' zone. Optimal zone, marked by the dashed rectangle, indicates the best choices of frequencies and phase difference considering all three metrics. The black point at the lower boundary of the zone denotes the parameters used by professional chefs.

as

$$\left(\boldsymbol{R}''_{\text{grain}}(\zeta, t) - \boldsymbol{R}''_{\text{wok}}(\zeta, t)\right) \cdot \boldsymbol{n}(\zeta, t) > 0. \tag{3.5}$$

Throughout the paper, the prime notation denotes the partial derivative with respect to time. Note that the take-off condition here only considers the kinematics. We thus model the rice as if it is a dry particle with no other attractive forces to the wok.

Using equation (3.5), we identify whether the rice takes off. Upon take-off, we assume negligible aerodynamic drag on the rice and no grain–grain collisions in the air. Therefore, upon take-off, the only external force on the rice grain is gravity, leading to the free-falling projectile motion

$$\boldsymbol{R}''_{\text{grain}}(\zeta, t) = [0, \ -g]. \tag{3.6}$$

At the beginning of the trajectory of the rice grain, the initial velocity and the position of the grain was set equal to the wok velocity and position at the take-off location. Using these conditions, equation (3.6) is integrated numerically (see the numerical simulation section that follows), until the rice grain falls back to the wok surface, often at a different location from the take-off point. Note that both rice grains and the wok centre move as a function of time. Thus, the landing position of the rice cannot be easily solved for analytically, but instead is calculated as the point where it first intersects a point on the wok. At the instant of landing, the rice grain is L away from the wok centre $\boldsymbol{R}_c(t)$. Accordingly, the landing condition may be written

$$|\boldsymbol{R}_{\text{grain}}(\zeta, t) - \boldsymbol{R}_c(t)| = L. \tag{3.7}$$

Given the landing position in Cartesian coordinates, we calculate the landing location in terms of the wok coordinate ζ_{landing}. For most of the cases that we studied, all the rice grains landed inside the wok ($|\zeta_{\text{landing}}| < \zeta_{\max}$) when the landing condition was satisfied. The 'failed catch' zone in figure 3 marks the exceptions.

3.3. Comparing wok tosses

We compare different stir-fry kinematics according to three metrics: the proportion of the rice going airborne p, the angular displacement of the rice grain $\Delta\zeta$ and the flight height of the grain h. The schematic of the metrics is shown in figure 3*a*. We do not have closed-form solutions for these metrics because the rice trajectory is calculated numerically. Instead, we discuss how each variable is calculated during our simulation.

To calculate the proportion p of rice leaving the wok, we monitor 201 sites on the wok over a period and calculate the proportion of sites that satisfy the take-off condition at least once. Given the dense distribution of jumping sites,

$$p = \frac{l_a + l_c}{l_a + l_b + l_c}, \tag{3.8}$$

where l_a and l_c are the width of the zones where rice jumps and l_b is the width of the dead zone, as shown in figure 3*a*.

The flying rice undergoes an angular displacement $\Delta\zeta$ measured from the wok centre. The angular displacement may be written as the angle along the wok between take-off and landing positions,

$$\Delta\zeta = \zeta_{\text{landing}} - \zeta_{\text{take-off}}. \tag{3.9}$$

The value of ζ may be obtained through coordinate transformation from kitchen coordinate (x,y) to the moving wok coordinate (ζ). We observe that rice from the wok's leftmost

side travels the furthest distance. Thus, for simplicity, we present results for rice leaving at this point, i.e. $\zeta_{\text{take-off}} = -\zeta_{\max}$. In our experiments, the chef's trajectories result in rice only launching from the left side of the wok, but other kinematics may have rice originating from both sides, as we will show in the results section.

The last metric we consider is the flight height, the largest distance achieved between the rice grain and the wok surface during the flight of the rice grain. This distance is measured along the line that intersects the rice grain and the closest point of the wok underneath it. Using geometry, this distance can be shown to equal the radius of the wok minus the distance between the rice grain and the wok centre,

$$h = L - \min_t \{|\boldsymbol{R}_{\text{grain}}(\zeta, t) - \boldsymbol{R}_c(t)|\}. \tag{3.10}$$

Our model of the rice trajectory is only valid after take-off and upon landing. In our experiments, we could not accurately trace the trajectories of the rice grains after landing due to the opacity of the wok. From our observations, the rice grains do not bounce upon landing. Instead, they experience inelastic collisions, losing most of their velocity perpendicular to the wok. The grains then slide to the left before being tossed in the next cycle. We do not attempt to model this interaction between the rice grain and the wok once landing has occurred.

3.4. Numerical simulation

We simulated the wok tossing process in Matlab. The trajectories of the points on the wok were calculated by calculating the time course of the angles θ_i from equation (3.1), which are in turn substituted into equation (3.2) to determine the Cartesian position of all points on the wok.

We simulated rice grain jumping from the 21 sites uniformly distributed on the wok bottom surface. Given the width of the wok in radians, the jumping sites had spacing 0.12 rad. We calculated the acceleration of the sites $\boldsymbol{R}''_{\text{wok}}(\zeta, t)$ by performing a second-order central difference scheme. At each time step, we examined whether the site satisfied the take-off condition, equation (3.5). In most cases, the sites in the middle of the wok failed to satisfy the take-off condition throughout the cycle. The centre of the wok can thus be considered a dead zone for fried rice and should be avoided.

Once equation (3.5) was satisfied, we simulated a rice grain particle taking off. The initial velocity and location of the rice grain is set by the motion of the wok. The trajectory of the rice grain $\boldsymbol{R}_{\text{grain}}(\zeta, t)$ is calculated by integrating the differential equation, equation (3.6). The time step of integration was set as $\Delta t = 0.002$ s, which is 0.6% of the period. Equation (3.6) was integrated using the explicit forward difference scheme.

For each rice grain, after the location and the velocity of the rice grains were updated at each time step, we checked whether the collision condition, equation (3.7), was satisfied. When the landing condition was satisfied, we stopped the integration for the particular rice grain trajectory and recorded the landing location ζ_{landing}. To show the trajectories of the rice grain relative to the wok, we transformed the trajectories from the kitchen frame to the wok frame.

Note that for any wok location there may be a window of time, consisting of several time steps, when the take-off condition, equation (3.5), is satisfied. We assumed that only one rice grain can take off from each site and that it takes off at the beginning of the take-off window. Therefore, we only calculated one rice trajectory per site.

4. Results

4.1. Kinematics of professional chefs

Wok tossing was divided into two stages, as shown in figure 1*b–e*. First, the chef pushed the wok forward and rotated it clockwise to catch the falling rice (figure 1*b*,*c*). Then, the chef pulled the wok back while rotating the wok counterclockwise (figure 1*d*,*e*) to toss the rice. At the beginning of the toss, rice grains are carried by the front end of the wok, which rises at a high velocity. Then, the wok switches direction and decelerates with nearly 1.5 times Earth's gravity, leaving the rice airborne and following projectile motion.

A unique feature of wok tossing is the see-sawing motion, as shown in electronic supplementary material, video S1 and figure 1. The left end travels in a clockwise circle while the right end moves in counterclockwise circle. How can a rigid body achieve such motion?

The key is using the stove rim as the fulcrum of the see-saw motion. We confirm that the wok maintains contact with the stove by tracking the centre of the osculating circle to the wok, shown by the red points in figure 1*b–e*. We refer to these red points as the wok centre. The wok centre has a constant distance from the stove rim, and this distance, 203 ± 3 mm, is close to the radius of curvature of the wok. Thus, the wok slides along the stove, but maintains contact. This key feature of wok stir-fry helps the chef to reduce the effort required to toss the food.

As shown in equation (3.2) and figure 2*a*, the kinematics of the wok may be described uniquely using a two-link pendulum with joint angles $\theta_i(t)$, which are in turn expressed by the six variables in equation (3.1). These variables include: the average angle of each pendulum $\bar{\theta}_i$, the amplitude of the pendulum motion A_i, the frequency of both pendulums f, and the offset phase angle between the pendulums ϕ. Through fast Fourier transformation of the position and angle of the wok for 17 consecutive tosses, we found the following values:

$$\left.\begin{aligned} \bar{\theta}_1 &= 0.3\,\text{rad}, \\ \bar{\theta}_2 &= 0.0\,\text{rad}, \\ A_1 &= 0.2\,\text{rad}, \\ A_2 &= 0.2\,\text{rad}, \\ f &= 3.0\,\text{Hz}, \\ \phi &= 1.0\,\text{rad}. \end{aligned}\right\} \tag{4.1}$$

These variables represent the kinematics of choice by professional chefs, and we will use these constants when we present predicted wok motions. We proceed by discussing these variables in turn and their impact on wok tossing performance.

Figure 2*c* shows the time course of the inclination angles θ_i for pendulum 1 and pendulum 2, shown in red and blue, respectively. The experiments are shown by the points. The theory, using equation (3.1) and values from equation (4.1), is shown by the solid lines. The fit is excellent for the three periods shown. Moreover, when the fit is done across 15 consecutive periods, we achieve an R^2 value of 0.93 and 0.98 for θ_1 and θ_2, respectively. A good fit is also shown in the kitchen coordinate (figure 2*b*), where the left and right ends of the

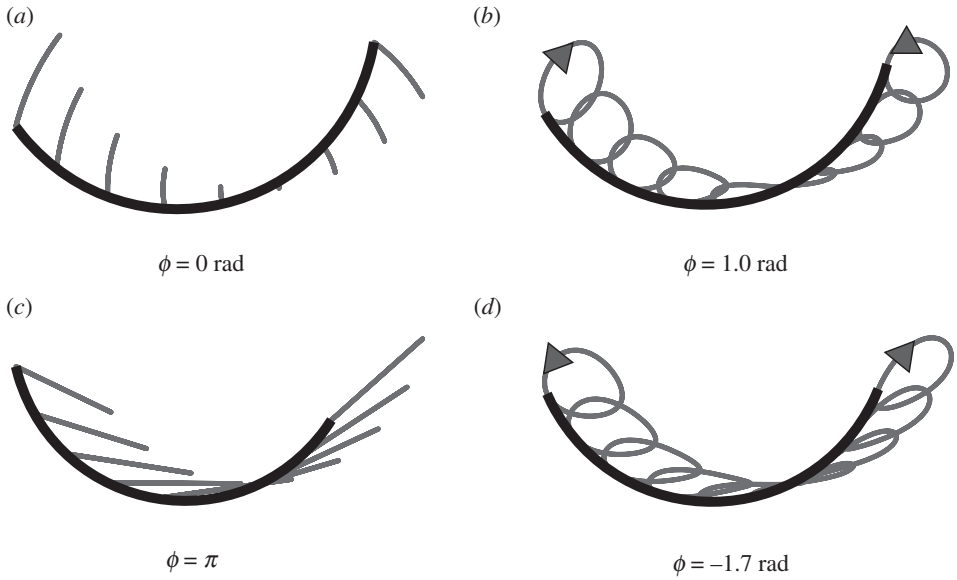

Figure 4. Simulated wok trajectories. Here, the trajectory of nine evenly spaced locations on the wok are shown as a function of phase difference ϕ. The phase difference $\phi^* = 1.0$ rad is used by professional chefs. In (*d*), a trajectory is shown that has a similar motion to the chef's chosen kinematics, but with a reversed direction.

wok are plotted in points and the theoretical trajectories, given by equation (3.2), are shown by solid lines.

Figure 2*d* shows the frequencies observed in our videos. In total, we collected data from five chefs cooking various stir-fry dishes. In one trial, we asked the chef to cook three servings of fried rice at the same time. Despite the variability in cooking conditions, we found the tossing frequency to be consistent at 2.7 ± 0.3 Hz ($N = 276$). Noticeably, when chefs toss the wok for many cycles in a row, the frequency also increases slightly. The variation is because the wok moves more slowly in the first few tosses before reaching steady state.

One reason for the chosen frequency is that the wok motion should synchronize with the rice falling through the air. If the wok has a much higher frequency than the frequency of rice landing, then energy is wasted. Conversely, if the wok tossing is at too low a frequency, then the rice remains immobile and could be burned. Indeed, the wok has a period of $T_{\text{cycle}} = 1/f = 0.33$ s. A distance of the wok radius represents approximately the furthest that rice would be thrown in the air and still feasibly caught. Using this distance, the time scale of rice falling is $\sqrt{2L/g} = 0.2$ s, which is of the same order as the wok period. The vertical grey bars in figure 2*c* show the periods that the rice is airborne, a value around 0.23 s, as calculated by the simulation in §3.2. From watching the experimental videos, we estimate this time scale to be 0.22 ± 0.02 s, which also matches the gravitational time scale.

The amplitudes A_1 and A_2 indicate the extent that the wok is moved back and forth, which leads to the wok's range of motion in figure 1*b–e*. The average angles $\bar{\theta}_i$ will also indicate the equilibrium position of the wok. We find that the chefs chose the values so that, on average, the wok is horizontal and is positioned to the left of the stove rim. This is mostly because the wok's handle is to the right of the stove rim.

The wok tossing speed will increase with increasing frequency and amplitude of the pendulums. However, the most important variable for wok tossing is the phase difference between the pendulums ϕ. This is because changing the phase differences leads to qualitatively different trajectories of the wok motion. We consider the different possible trajectories in turn below.

4.2. Simulating all possible kinematics and rice trajectories

We first consider the two pendulums in phase. Here, $\phi = 0$ and the angle between the two pendulums, $\theta_1(t) - \theta_2(t)$, is constant. In this scenario, the back and forth motion of the wok disappears, and only the rotational motion remains. In other words, the wok simply rocks back and forth like a see-saw around a single non-moving fulcrum. The traces of the points on the wok are simply arcs of circles, as shown in figure 4*a*. The problem with this motion is that each rice grain mainly travels up and down, as shown by the arrows in the figure. With just vertical motion, there is little mixing of the rice. The rice in the middle of the wok remains stationary, leading to it being overcooked. Conversely, the rice on the outside rims may be undercooked.

At the other extreme, if $\phi = \pi$, the two pendulums are 180° out of phase. Here, the wok is mainly sliding left and right, as shown by the nearly horizontal trajectories of the wok in figure 4*c*. This is also unfavourable because there is no vertical motion of the wok surface. Thus rice will not jump and the airborne time of the rice will be limited, leading to insufficient cooling before the rice falls back down to the wok.

The phase difference chosen by the chefs, $\phi^* = 1.0$ rad, is between the $\phi = 0$ and $\phi = \pi$ zones, which leads to the key feature of the stir-fry process: a combination of both vertical and horizontal trajectories of the wok. Consistent with the wok motion, the rice follows elliptical trajectories, as shown in figure 4*b*. Moreover, the best trajectories are at the outermost portions of the wok, where the wok is moving the greatest vertically. The bottom of the wok exhibits a dead zone, where trajectories are mostly horizontal. Such a zone may serve a purpose: the centre of the wok is like a catcher's mitt in baseball, i.e. when the rice grains land there, they lose most of their kinetic energy because of the collision. In experiments, the wok slides to the right after the rice lands. The inertia of the rice and the slippery wok surface result

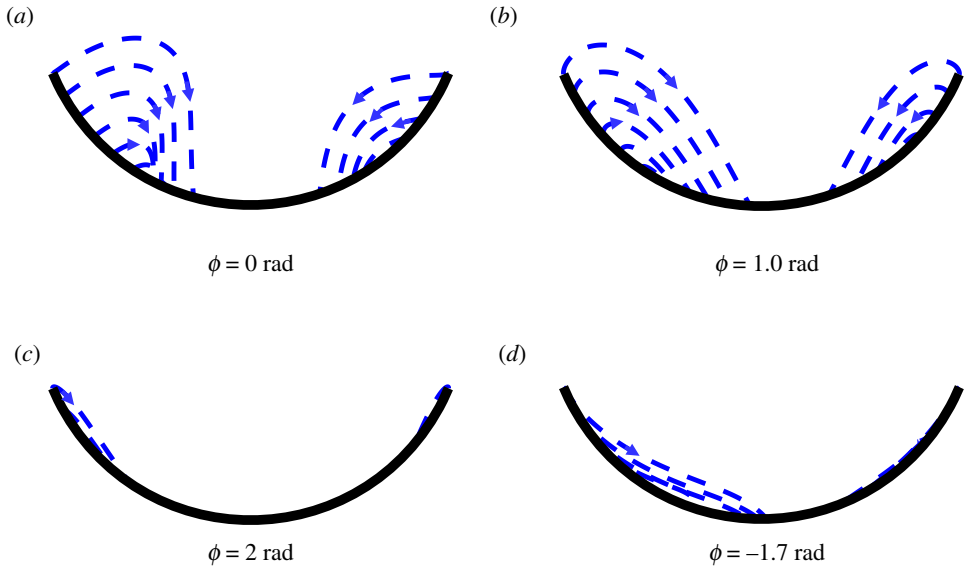

Figure 5. Simulated rice trajectories using 20 sites uniformly spread on the wok surface. The phase angle $\phi^* = 1.0$ rad is used by professional chefs. Little jumping was observed when $\phi = 2$ rad.

in the rice sliding to the left edge of the wok, ready to be thrown up again.

The last regime we will consider is wok trajectories with a negative phase difference. This is demonstrated for $\phi = -1.7$ rad in figure 4*d*. The trajectories are elliptical, as in the previous case of chef tossing, but the motion of the wok is reversed. The left end of the wok moves counterclockwise while the right end moves clockwise. Indeed, in equation (3.1), if we substitute t with $-t$ and ϕ with $-\phi$, the same θ_i values will be obtained. This means that the motion is reversed by choosing $\phi^* = \phi$, while maintaining the same trajectory. Although the trajectory of the wok travels the same paths, the direction travelled does make a difference in terms of the motion of the grains. This is because gravity remains a fixed direction. As we will see later in our phase diagrams of tossing metrics, symmetry is broken when the interaction between the rice grains and wok is considered.

Now that we have characterized how the wok trajectories change with the phase ϕ, we use our projectile simulation to predict the corresponding trajectories of the rice. Although the wok is moving, the trajectories are shown according to the coordinate frame fixed to the wok, as shown in figure 5. We will use the trajectories of rice to infer which wok tossing strategies are optimal. Electronic supplementary material, video S2 shows our numerical predictions for the trajectories of rice grains using the chef's choice of phase difference $\phi^* = 1.0$ rad. Rice grains that take off from different locations on the wok have trajectories that cross each other, indicating good mixing.

In our previous analysis, we saw that the phase angle $\phi = 0$ led to mostly vertical oscillation of points on the wok. This high vertical velocity leads to rice trajectories with large heights, as shown in figure 5*a*. This is because most of the wok satisfies the take-off condition (equation 3.5) at some time point in the cycle period. However, we observe a large dead zone at the bottom of the wok as the take-off condition is never satisfied there.

At the chef's phase difference $\phi = 1.0$ rad, the rice grains travel a longer horizontal distance at a compromise of reaching a shorter height. As indicated in figure 3*b*, the rice grain travels as far as $\Delta\zeta = 1.1$ rad, which is almost half of the wok. This indicates that more mixing is possible than with $\phi = 0$.

As expected, as the phase angle increases, the trajectories become less favourable. Figure 5*c* shows the rice trajectories for $\phi = 2$ rad. Here, little jumping is possible because the wok motion is mostly horizontal. Indeed, equation (3.5) implies that horizontal acceleration is not beneficial for jumping. Instead, the wok has to undergo a vertical downward acceleration greater than g for take-off to happen, as the normal direction of the wok is mostly vertical. Although horizontal and vertical acceleration will take the same energy from the chef, its the correct combination of both that will launch rice from the wok.

An elliptical wok trajectory does not necessarily imply good jumping behaviour. When $\phi = -1.7$ rad, the wok positions trace out ellipses as shown in figure 4*d*, yet the rice does not jump as well (figure 5*d*). This is due to the complex interaction between the rice trajectory and wok motion. When $\phi = -1.7$ rad, rice jumps mostly horizontally to the right, resulting in early landing on the wok surface. When $\phi = -1.0$ rad, despite having the same elliptical trajectory as figure 4*b*, the rice trajectories are distinct. Electronic supplementary material, video S3 shows that, when the motion is reversed, rice grains do not always jump from left to right. Instead, grains close to the bottom of the wok jump towards the left. This will lead to collisions of rice grains, which we did not simulate. Thus, an elliptical trajectory is necessary but not sufficient for jumping.

4.3. Metrics for evaluating wok tossing

The previous image sequences of wok and rice trajectories indicate that the motion of the rice is highly dependent on the phase angle ϕ. To better explore this space and to determine the optimal wok tossing kinematics, we consider three metrics. These metrics include the proportion p of the wok that satisfies the take-off condition, angular displacement of rice $\Delta\zeta$ and flight height h of the rice. Except for the proportion of the wok that satisfies detachment, the other metrics are calculated by considering the leftmost point of the wok, which launches the rice the furthest.

The phase diagrams for these metrics are shown in figure 3*b–d* as a function of frequency and phase difference.

Generally, yellow regions of the plot indicate better performance, as shown in the legend. The parameters pertaining to the chef's tossing, $f^* = 3.0$ Hz and $\phi^* = 1.0$ rad, are indicated by the black points in the three regime diagrams. The optimal region is marked by the dashed lines, and was estimated based on the intersection between the yellow zones in all three plots. The no-flight zone, a region associated with stationary rice grains that cannot jump, is shown in grey, and generally occurs for woks tossed with insufficient frequency ($f < 2$ Hz). Finally, we defined a 'failed catch' zone, where rice grains that jumped from the left end fail to land in the wok. This zone lies in large frequency and small phase difference.

Figure 3*b* shows the proportion p of the wok that satisfies the take-off condition at least once in a cycle. This figure is bilaterally symmetric because of the similarity in the trajectory of the wok for phase differences $\phi < \pi$ and $\phi > \pi$, as we have previously shown in figure 4*d*. In order to toss a larger proportion of the wok's rice grains, chefs should choose large frequency and small phase difference magnitudes (small $|\phi|$). For these locations, almost 40% of the wok can achieve take-off of rice. It is the hardest for the rice grains to jump when $\phi = \pi$, regardless of the frequency.

Figure 3*c*,*d* shows the angular displacement and the flight height of the rice grains. Angular displacement $\Delta\zeta$ is reported in units of radians, and represents the difference in angular position of the take-off and landing position of the rice. This idea is analogous to an aeroplane flying from one longitude to another. This value gives an idea of the time that the rice is in the air. The maximum possible angular displacement is $2\zeta_{max} = 2.4$ rad, or the entire extent from the left- to the right-hand side of the wok. If $\Delta\zeta > 2\zeta_{max}$, it would mean that the rice has jumped over the right edge of the wok. This happens under high frequency $f > 7$ Hz and small $|\phi|$ values.

When the frequency is fixed at 3.0 Hz, there appear two optimal choices of ϕ that enable the rice grain to land the furthest. One is at $\phi = 1.0$ Hz, which is the chef's choice of phase difference, and is demarcated by the dashed optimal region. The other that appears optimal is around $\phi = -1.7$ Hz. Note that the yellow region around $\phi = 1.0$ Hz is wider than the one around $\phi = -1.7$ Hz, indicating more tolerance for variability by the chef. Why do chefs not choose the other optimal zone, associated with $\phi = -1.7$ Hz? We can gain insight by considering the rice trajectories shown in figure 5*d* and the flight height shown in figure 3*d*. Rice grains travel an appreciable distance, but their flight height is limited. Thus, we conclude that there is a single optimal zone, associated with the chef's parameters, of $f = 3.0$ Hz and $\phi = 1.0$ Hz.

Figure 3*d* shows the height in millimetres for the peak of the rice's jump. We define the height as the distance between the rice grains and the location on the wok that is the closest to them. Therefore, owing to the circular geometry of the wok, this metric has to be smaller than or equal to the wok radius L, or 200 mm. This is consistent with experiments because the rice is almost always caught by the wok. Chefs should avoid using phase differences $\phi > \pi$, because they are associated with lower flight heights and less cooling of the rice.

To compare the simulation with the experiment in a more quantitative way, we measured the maximum jump height of the rice grains in the kitchen coordinate in each toss. The experimental data suggest that the grains may be tossed to a height of 218 ± 8 mm above the stove rim. In electronic supplementary material, video S2, we see that the simulation predicts the rice to be tossed to a maximum height of around 170 mm from the wok. The simulation value is slightly lower than the observed value because it is a better representation of an averaged behaviour of rice grains that take off at around the same time. Indeed, as we can observe in the electronic supplementary material, video S1, most of the rice grains are not able to jump quite as high as the highest one.

Considering all three metrics, the zone marked by the dashed lines is the global optimum. We suggest that chefs or machines should increase frequency to enable the rice grains to jump to greater heights and travel larger distances. This might enable the rice to be cooked at even higher temperatures or over shorter cooking times. Such high frequencies have several downsides. At too high a frequency, the rice may approach the failed catch zone, causing food to be wasted. Furthermore, tossing at a higher frequency would require substantially more power use by the chefs. The power required is the product of force and velocity, which scale with f^2 and f, respectively. Thus power $P \sim f^3$, and doubling the frequency would require eight times as much power. The power will also increase linearly with the amount of food cooked. Thus, cooking large amounts of fried rice or cooking fried rice more quickly would be best done with automated cooking robots.

Lastly, we depart from wok kinematics by exploring whether stir-fry cooking can be improved through optimizing wok geometry. We evaluate the rice jumping behaviour under different wok shapes, ζ_{max}. A smaller ζ_{max} represents a larger aspect ratio D/W of the wok. We fix the wok kinematics by fixing the frequency and phase difference ϕ. By increasing ζ_{max}, the rice grains can have more area to jump from. However, as we show in figure 6 and electronic supplementary material, video S4, rice grains can only take off from a certain region of the wok even when ζ_{max} is very large.

The most shallow wok sees very little jumping, as shown in figure 6*a*. Figure 6*b* shows the wok that chefs use, which displays great jumping performance. A very deep wok, such as the one shown in figure 6*c*, has an even larger area from which rice can jump. However, it also has more dead zones: rice grains cannot take off from the vertical portion of the wok. Figure 6*d* shows that, as the wok size increases from a small value, rice grains taking off from the left end of the wok are able to land further to the right portion of the wok (red line). This trend plateaus when the wok takes the shape of a semicircle, $\zeta_{max} = \pi/2$. A further increase in wok size ζ_{max} cannot increase the effective area of rice grain tossing.

The current value of $\zeta_{max} = 1.2$ rad lies in the region where increasing wok size would enable rice grains to jump further. Thus, it appears that a larger wok might provide benefit for cooking more rice. We speculate that other reasons that we did not consider have limited wok size. For example, a taller wok may require the use of a spatula to transport the rice grains back towards the left.

5. Discussion

In this study, we neglected three-dimensional motion, which we briefly discuss now. In our observations of chefs, we saw that falling rice tends to slide towards the centre. A wok shaped like a spherical section acts like a catcher's mitt, causing off-centre grains to aggregate together. Aggregating food in the centre makes the rice trajectories more predictable, which helps to catch the rice grains after they have been launched. It also helps to mix the ingredients together,

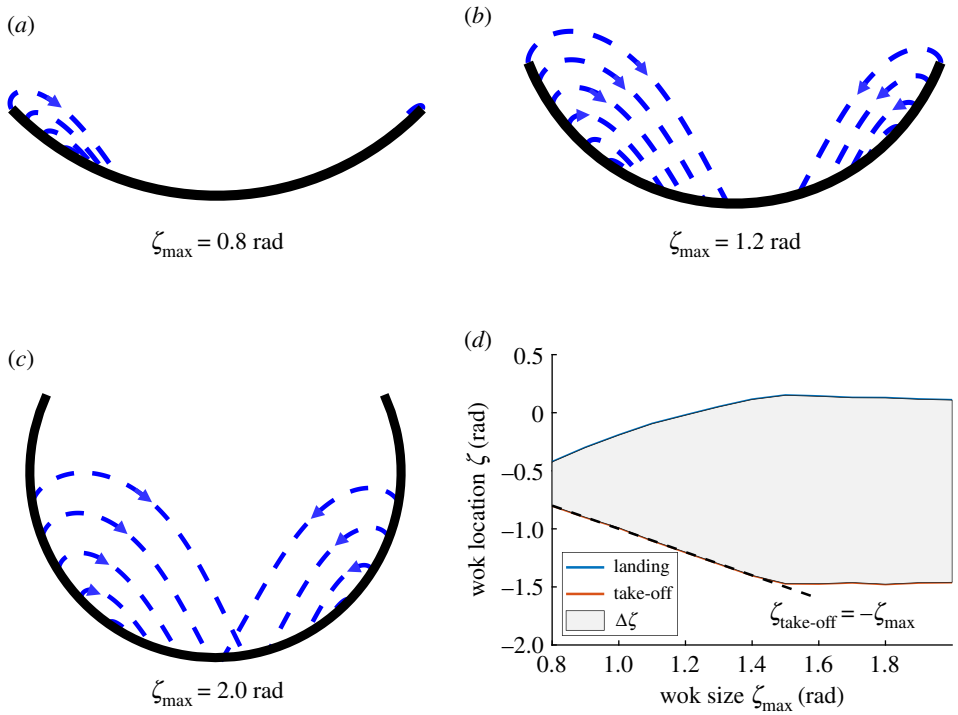

Figure 6. Effect of wok shape on the rice trajectory. (*a–c*) More rice grains may be tossed as the wok becomes deeper. (*d*) The relationship between wok shape ζ_{max} and the take-off and landing location of the furthest jumping grain. When the wok size is below 1.5 rad, the furthest rice grains take off from the leftmost end, thereby coinciding with the line $\zeta_{take\text{-}off} = -\zeta_{max}$.

which leads to even cooking. Using two-dimensional kinematics to cook simply makes it easier for the chef to toss the wok. However, the three-dimensional shape of the wok is important in practice. A wok shaped like a trough would not experience the aforementioned benefits.

This study focused on using wok motion alone to move rice. However, in practice, chefs often employ other implements such as a spatula, which weighs much less than the wok. The spatula transports ingredients from the bottom of the wok to the jumping zone at the edge. The spatula also breaks up larger chunks of ingredients and prevents food from sticking to the wok. Nonetheless, our analysis indicates that the primary reason for the take-off of rice is the motion of the wok.

This study might inspire the construction of large-scale cooking machines. On the opening day of the 2008 Beijing Olympics, as much as 3000 kg fried rice was consumed in the Olympic village. The Guinness World Record for the largest serving of fried rice is held by the Turkey Culinary Federation, which made fried rice that weighed 3150 kg in 2014 [23]. It took 20 chefs each 5 h to finish the task. Although cooking in big batches is strenuous for chefs, it can potentially reduce heat losses by having a relatively smaller surface open to the air per unit weight. Thus, large-scale cooking has the potential to save energy, especially for large numbers of customers. In our recordings, making three servings of fried rice took only 25% more time than one serving. Considering the high energy consumption of the propane burner at around 30 kW, cooking in even larger quantities may save even more fuel.

The model we present in this paper may be useful in industrial applications. Uniform mixing and heating are critical for making granular foods such as popcorn [24]. Outside of the food industry, granular mixing with heat addition is heavily involved in biomass plants [25]. Particle mixing performance is also important for the pharmaceutical industry [26]. In general, the methods used in the industry to mix materials are limited and granular mixing remains an active area of research [27,28]. We envision that wok tossing kinematics will become a more effective alternative to the traditional rotating drum methods used in current automated cooking machines. In the meantime, our study enables further research on designing a wearable device to reduce the burden on chefs.

6. Conclusion

We developed a mathematical model that successfully described the wok tossing process. Tossing is a combination of two independent motions, a side to side motion and a see-saw motion, allowing rice grains to slide around the wok as well as to jump off the surface. We identify two critical parameters that chefs can vary: the frequency of tossing and the phase lag between the two motions applied. By filming professional chefs, we found that, at the frequency chosen by chefs, the phase difference performed is optimal for mixing. We suggest that future chefs increase the frequency of motion, which may enable rice to jump further, and promote cooling and mixing.

Ethics. Since identifiable human features were not recorded in the videos, IRB review and approval were not necessary for this study.

Data accessibility. Data on the frequency calculations are included in the electronic supplementary material, table S1. The main video we used for kinematics measurement is included as video S1 in the electronic supplementary material.

Authors' contributions. H.K. collected data, built the mathematical model, performed the numerical analysis and drafted the manuscript. D.L.H. and H.K. conceived, designed and coordinated the study and helped draft the manuscript. Both authors gave final approval for publication.

Competing interests. We declare we have no competing interest.

Funding. This work was supported by D.L.H.'s CAREER award from the National Science Foundation (PHY-1255127).

Acknowledgements. We want to acknowledge Taitung County Chulu Junior High School for lending us the video recorders. We also thank Yukai Sun for providing the tossing frequency data from China.

References

1. Wilkinson EP. 2012 *Chinese history: a new manual*, vol. 84. Cambridge, MA: Harvard University Asia Center.
2. Kraig B, Sen CT. 2013 *Street food around the world: an encyclopedia of food and culture*. Santa Barbara, CA: Abc-clio.
3. Young G, Richardson A. 2004 *The breath of a wok: unlocking the spirit of Chinese wok cooking through recipes and lore*. New York, NY: Simon and Schuster.
4. Maillard LC. 1912 Action des acides amines sur les sucres; formation des melanoidines par voie methodique. *Comptes R. Acad. Sci. (Paris)* **154**, 66–68.
5. Myhrvold N, Young C, Bilet M. 2015 *Modernist cuisine*. Bellevue, WA: The Cooking Lab.
6. Xu YW, Cheng ASK. 2014 An onsite ergonomics assessment for risk of work-related musculoskeletal disorders among cooks in a Chinese restaurant. *Work* **48**, 539–545. (doi:10.3233/WOR-131805)
7. Tsai J. 2009 Chinese immigrant restaurant workers' injury and illness experiences. *Arch. Environ. Occup. Health* **64**, 107–114. (doi:10.3200/AEOH.64.2.107-114)
8. Chyuan JY. 2007 Ergonomic assessment of musculoskeletal discomfort among commissary foodservice workers in Taiwan. *J. Foodserv. Bus. Res.* **10**, 73–86. (doi:10.1300/J369v10n03_05)
9. Liu Lw, Wang Ah, Hwang Sl, Lee Yh, Wang Ah, Hwang Sl, Lee Yh. 2011 Prevalence and risk factors of subjective musculoskeletal symptoms among cooks in Taiwan. *J. Chin. Inst. Ind. Eng.* **0669**, 327–335.
10. Kormushev P, Calinon S, Caldwell DG. 2010 Robot motor skill coordination with EM-based reinforcement learning. In *Proc. 2010 IEEE/RSJ Int. Conf. on Intelligent Robots and Systems, Taipei, Taiwan, 18–22 October 2010*, pp. 3232–3237. New York, NY: IEEE.
11. Bollini M, Tellex S, Thompson T, Roy N, Rus D. 2013 Interpreting and executing recipes with a cooking robot. In *Experimental robotics 2013*, pp. 481–495. New York, NY: Springer International Publishing.
12. Beetz M, Klank U, Kresse I, Maldonado A, Mösenlechner L, Pangercic D, Rühr T, Tenorth M. 2011 Robotic roommates making pancakes. In *Proc. 11th IEEE-RAS Int. Conf. on Humanoid Robots (Humanoids 2011), Bled, Slovenia, 26–28 October 2011*, pp. 529–536. New York, NY: IEEE.
13. Zhai J, Yan W, Fu Z, Zhao Y. 2012 Kinematic analysis of a dual-arm humanoid cooking robot. In *Proc. of 2012 IEEE Int. Conf. on Mechatronics and Automation, Chengdu, China, 5–8 August 2012*, pp. 249–254. New York, NY: IEEE.
14. Wang TJ. 1957 *Automatic cooking device*. US Patent no. 7,485,830.
15. Lee YC, Lee WL. 1987 *Automatic frying machine*. US Patent no. 4,700,617.
16. Chapin RA. 1985 *Method and apparatus for automated Chinese stir-fry cooking*. US Patent no. 4,503,502.
17. Yan WX, Fu Z, Liu YH, Zhao YZ, Zhou XY, Tang JH, Liu XY. 2007 A novel automatic cooking robot for Chinese dishes. *Robotica* **25**, 445–450. (doi:10.1017/S0263574706003250)
18. Wong H, Zhou PW. 1992 *Automatic food cooking device*. US Patent no. 5,088,390.
19. Wong GS. 1995 *Automated cooking apparatus*. US Patent no. 7,930,973.
20. Farid MS, Knight BE, Shulueter LS, Rogers KT, Ubellacker WL, Seidell SN. 2015 *Automated meal production system and apparatus*. US Patent no. 10,154,762.
21. Li C. 2014 *Fully automated stir-fry machine*. China Patent no. 203417090U.
22. Schneider CA, Rasband WS, Eliceiri KW. 2012 NIH Image to ImageJ: 25 years of image analysis. *Nat. Methods* **9**, 671. (doi:10.1038/nmeth.2089)
23. Glenday C. 2015 *Guinness world records 2015*. New York, NY: Bantam.
24. Virot E, Ponomarenko A. 2015 Popcorn: critical temperature, jump and sound. *J. R. Soc. Interface* **12**, 1–6. (doi:10.1098/rsif.2014.1247)
25. Brown JN, Brown RC. 2012 Process optimization of an auger pyrolyzer with heat carrier using response surface methodology. *Bioresour. Technol.* **103**, 405–414. (doi:10.1016/j.biortech.2011.09.117)
26. Muzzio FJ, Shinbrot T, Glasser BJ. 2002 Powder technology in the pharmaceutical industry: the need to catch up fast. *Powder Technol.* **124**, 1–7. (doi:10.1016/S0032-5910(01)00482-X)
27. Ottino JM, Khakhar DV. 2000 Mixing and segregation of granular materials. *Annu. Rev. Fluid Mech.* **32**, 55–91. (doi:10.1146/annurev.fluid.32.1.55)
28. McCarthy JJ, Khakhar DV, Ottino JM. 2000 Computational studies of granular mixing. *Powder Technol.* **109**, 72–82. (doi:10.1016/S0032-5910(99)00228-4)